

An Undergraduate Analysis of the Mars 2020 Entry, Descent, and Landing

Robert Vandergriff¹

University of Tennessee Knoxville, Tennessee 37996

Harrison Shay²

University of Tennessee Knoxville, Tennessee 37996

Lilanie Abdur-Rahman³

University of Tennessee Knoxville, Tennessee 37996

Jesse Groves⁴

University of Tennessee Knoxville, Tennessee 37916

With each iteration of the Mars science laboratory (MSL) missions, there are new additions to the Mars entry vehicle aimed at gathering more data or making the mission more efficient. Although many of the improvements are geared towards enhancing surface exploration, there is an equal amount of attention paid to the function of the flight vehicle. This part of the mission, known as entry descent and landing, is constantly evolving as computational fluid dynamics, ground testing and flight data becomes more available. This is a review of the hypersonic and aerothermal data of the MSL Mars missions of 2012 and 2020. It closes with a look towards future ground testing and computations fluid dynamic models.

I. Nomenclature

<i>EDL</i>	=	Entry Decent Landing
<i>EI</i>	=	Entry Interface
<i>MEADS</i>	=	MEDLI2 Entry Atmospheric Data System
<i>MEDLI</i>	=	Mars Entry, Descent, and Landing Instrumentation
<i>MEDLI2</i>	=	Mars Entry, Descent, and Landing Instrumentation 2
<i>MISP</i>	=	MEDLI2 Instrumented Sensor Plug
<i>MPB</i>	=	MEDLI2 Pressure Backshell
<i>MPH</i>	=	MEDLI2 Pressure Heatshield
<i>MSL</i>	=	Mars Science Laboratory Mission
<i>MTH</i>	=	MEDLI2 Thermal Heatshield
<i>PICA</i>	=	Phenolic Impregnated Carbon Ablator
<i>RCC</i>	=	Reinforced Carbon Carbon
<i>TPS</i>	=	Thermal Protection System
<i>M</i>	=	Mach Number
<i>P</i>	=	Static Pressure
<i>P_t</i>	=	Total Pressure
<i>T</i>	=	Static Temperature
<i>T_t</i>	=	Total Temperature

¹ Student, MABE.

² Student, MABE.

³ Student, MABE.

⁴ Student, MABE.

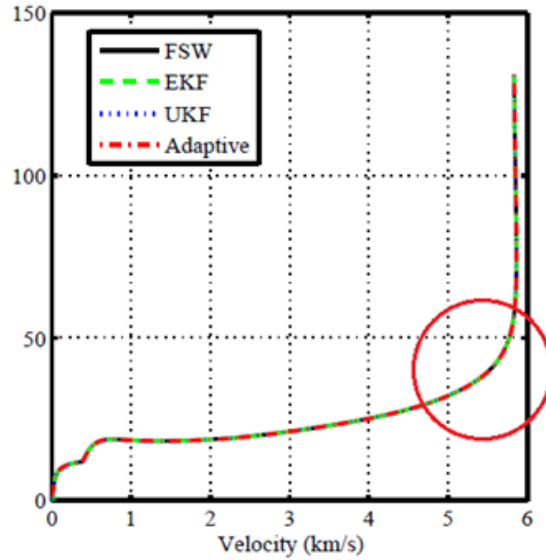
II. Introduction

There will always be an innate curiosity and desire to learn more within humans. This desire to learn includes learning about space as well. With this desire to learn more about space and our solar system, humans started by reaching the moon, and many people have now looked to Mars in search of answers. Mars is the next logical step in exploring the solar system because of its favorable conditions for astronauts and equipment compared to the two closer planets, Mercury and Venus [1]. Along with learning more about Mars, studying Mars could help scientists better understand what happens here on Earth. In order to reach Mars, there are a lot of factors that need to be considered. One example of this is that Mars is an average of 140 million miles away from Earth [2]. This means to reach Mars within a reasonable time, the spacecraft must be moving really fast. After considering all of these factors, it is important to understand how the capsule will react to these very intense conditions. An example of this would be extreme temperatures due to drag in the atmosphere while moving at very high speeds. The most common ways to measure all of this data to help design the capsule in such a way that it is best suited for the mission are wind tunnel experimentation, flight testing, and numerical investigations. This paper will cover a proposed mission to Mars in which a rover will be sent to study the surface of Mars. For this mission, the details about the proposed flight path and conditions the capsule will need to endure during its flight, such as pressures and temperatures on the capsule, Mach numbers, etc., will be discussed along with the design challenges that correlate to these parameters. The paper will also cover these potential aerodynamic phenomena that could impact the mission, and the design challenges that these phenomena present. Lastly, this paper will go over the different types of ground testing and CFD work recommended to get a better understanding of how the capsule will react in these conditions. This will include what types of wind tunnels, gasses used in the wind tunnels, and the specific wind tunnels in the country recommended to be used for this ground testing.

III. Flight Path and Mission

The mission to Mars is extremely difficult and characterized by many risks where everything needs to go according to plan. There are many different aspects to the trip, however it has been said that the most crucial and risky are the 7 minutes where the module enters the atmosphere and lands on the surface of Mars. This is due to the extreme speeds and conditions the module experiences during the entry, descent, and landing (EDL) phase of the trip. This section of the lab will focus on the path and steps taken during this phase as well as some analysis on the conditions experienced by the module.

Since this section of the mission is characterized by high risk, there are many different stages to ensure a safe landing. First, the module separates from the cruise ship that it rode with on its trip to Mars. After that the capsule will complete final steps to adjust the heat shield before entering the atmosphere. The capsule entered with an angle of attack of approximately 16° . Once the capsule enters the Martian atmosphere it will experience peak heating and deceleration quickly. The peak heating will happen approximately 85 seconds after atmospheric entry. Peak deceleration happens about 10 seconds after that [4]. The peak deceleration will slow the module down to approximately 420 m/s. The velocity with respect to altitude for the Mars 2020 mission is shown in the figure below.



(a) Altitude vs. velocity

It can be observed in this diagram the peak deceleration at approximately 35km within the red circle. This report will primarily focus on the conditions and events during this period of the flight due to the extreme conditions. However, after this section of the flight the capsule is slow enough to deploy the supersonic parachute. This will further decrease the speed of the module. Approximately 20 seconds after the parachute deploys the heat shield will separate from the rover. This will allow the rovers' cameras and sensors to locate the landing site. The rover will then separate from the parachute and use rocket propulsion to lower itself to the surface [4]. The rover landing on the ground marks the end of the 7 minutes of terror of the EDL phase of the mission.

In this report, the team calculates the predicted flight conditions the capsule will experience. For this analysis, the peak heating and deceleration phases will be focused on since those are characterized by the most extreme conditions. More specifically, two altitudes were chosen for the analysis, these are at 35km and 50km. At these altitudes the free stream static temperature, pressure, and density will be used from [5]. These are the predicted values during the Mars 2020 landing. The following table shows the free stream static temperature and pressure for their respective altitude used in the analysis.

Condition	35km	50km
Temperature (K)	172.166	154.729
Pressure (Pa)	17.22	2.646
Mach number	25.65	27.09

To calculate the total values for the flight environment, isentropic relations will be used. The total temperature and pressure can be calculated using the respective equations.

$$T_t = T * \left(1 + \frac{\gamma - 1}{2} M^2\right)$$

$$P_t = P * \left(1 + \frac{\gamma - 1}{2} M^2\right)^{\frac{\gamma}{\gamma - 1}}$$

The following table shows the predicted total temperature and pressure for the flight environment at the respective altitude.

Condition	35km	50km
Total Temperature (K)	17211.38	17139.45
Total Pressure (Pa)	7.88*	1.94*

For this analysis the static temperature and pressure on the heat shield were also approximated. During the entry and descent of the module in the Martian atmosphere, a normal shock develops a distance off from the heat shield [7]. Knowing this, the static temperature and pressure can be calculated on the other side of the normal shock using the normal shock relations. These are shown by the equations below [8].

$$T_2 = T_1 * \left(\frac{((2 * \gamma * M^2) - (\gamma - 1)) * ((\gamma - 1)M^2 + 2)}{(\gamma + 1)^2 M^2}\right)$$

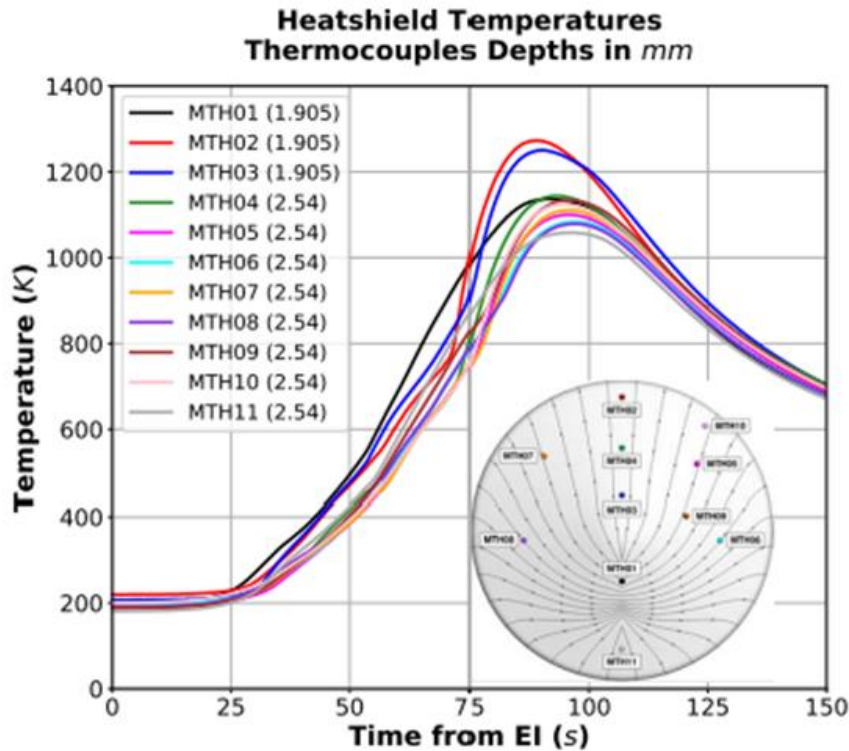
$$P_2 = P_1 * \left(\frac{2 * \gamma * M^2 - (\gamma - 1)}{\gamma + 1}\right)$$

The following table shows the resultant static pressures and temperatures after the normal shock along the heat shield of the module.

Condition	35km	50km
Static Temperature (K)	16842.05	16883.56
Static Pressure (Pa)	12804	2194

Across the shock wave the temperature and pressure increase. On the Mars 2020 mission, thermocouples were put into the heat shield in strategic placing. The report talks about the thermocouples in more detail in a later section. However, the thermocouple measured the static temperature along the heat shield. This data is shown in the

graph below. This data is from [12].



As it can be seen in the graph above, the max temperature read by the thermocouples is somewhere around 1300K. This is less than what was calculated for the prediction which is around 16800K. There are a few reasons why this error could be happening. First, at speeds such as Mach 25.65 and 27.09 the real gas law becomes less applicable. At these speeds, some of the energy dissipates into changing the molecules around it and being stored in bonds between molecules. Also, some of the energy dissipates into radiation. These effects are explained in further depth in the aerothermodynamic phenomenon section. Other reasons for this error could be the location of the measurement in conjunction to where the calculation conditions are. The thermocouples are a couple of mm inside of the heat shield. Whereas the static temperature will be directly on the other side of the normal shock.

More values were calculated as part of the analysis to predict the flight conditions. These values include Sutherland's Viscosity, speed of sound, Reynolds number per length, and the total enthalpy. These are shown in the table below.

Condition	35km	50km
Sutherland's Viscosity (kg/ms)	0.00001099	0.000009805
Speed of Sound (m/s)	207.6	196.5
Velocity (m/s)	5325	5325

Re/x	254000	48680
Total Enthalpy (J/kg)	14320000	14310000

IV. Aerodynamic Phenomena

The Martian atmosphere is remarkably different than that of Earth's, with a majority composition of Carbon Dioxide, and almost ten times smaller in width. **Table 1** shows the percent composition of the dominant gases on Earth and Mars [10]. This creates a difference in aerothermodynamic phenomena that occur during entry. Traveling at over 10,000 mph, the spacecraft hits the Martian atmosphere with a spectacular amount of energy. The drag produced by the particles that make up the Martian atmosphere drastically slows down the craft turning mass amounts of kinetic energy into mass amounts of thermal energy, which in turn creates extreme temperatures. The kinetic energy is turned to thermal energy by a process called adiabatic heating. The peak heating from the drag occurs approximately 80 seconds after entering the atmosphere and reaches temperatures of over 2000 K on the exterior [13]. The energy that the craft experiences can reach up to thirteen megajoules per kilogram which is enough to vaporize any material known to man which is why spacecrafts are designed to absorb as little energy as possible.

Table 1: Martian Atmospheric Composition.

Dominant Gases	Mars (%)	Earth (%)
Carbon Dioxide (CO_2)	95.0	.0391
Nitrogen (N)	3.00	78.1
Argon (Ar)	1.60	.930
Oxygen (O_2)	.174	20.9

As the craft enters the Martian atmosphere at hypersonic speeds, the particles comprising the atmosphere cannot relocate quick enough. Since the particles cannot relocate quick enough, the particles begin to ionize into a superheated plasma. This results in a shockwave around the nose of the vehicle which can reach temperatures of up to 20000 K. However, the shockwave does not occur directly on the surface of the craft because of a boundary layer between the surface of the craft and the shockwave which stays around 2-6000 K. The boundary layer is empirical to the survival of a spacecraft during atmospheric entry. Therefore, to keep the shockwave as far away as possible from the surface of the craft, crafts are designed with boundary layers in mind. For most spherical crafts, the distance from the shockwave to the surface is roughly proportional to the radius of the sphere. Thus, most craft are designed with blunt features to increase the radius between the surface and the shockwave. The majority of the heat created is witnessed on the impact surface, but the thermal radiation does heat the back of the craft as well. The superheated shockwave that occurs has a high enough temperature and pressure to cause the surrounding particles to dissociate into a superheated plasma by a process called ionization. For a hypersonic entry to the Martian atmosphere, plasma is created, compared to plasma for Earth's atmosphere because of the difference in composition. Most of this superheated plasma is pushed away by the boundary layer into the surrounding atmosphere leaving fantastic reentry trails Fig. 1 [14].



Fig. 1: Reentry Particle Effect.

A heat shield might react differently to the nitrogen rich atmosphere of Mars than to that of Earth's oxygen rich atmosphere. Therefore, the chemistry of the Martian atmosphere is important to consider before deciding materials of the heatshield. The dissociating ions around the craft not only create energy but also undergo reactions on and around the surface of the craft. When the reactions occur on the craft, the surface acts as a sort of catalyst and at times the reactions can chemically attack the heat shield by oxidation. Both Earth and Mars currently have an oxidizing atmosphere instead of reducing. However, the reactions causing oxidation can be used to an advantage by a process of ablation. Fig. 2 shows an image of an ablating material and the boundary layer created by escaping gases [11].

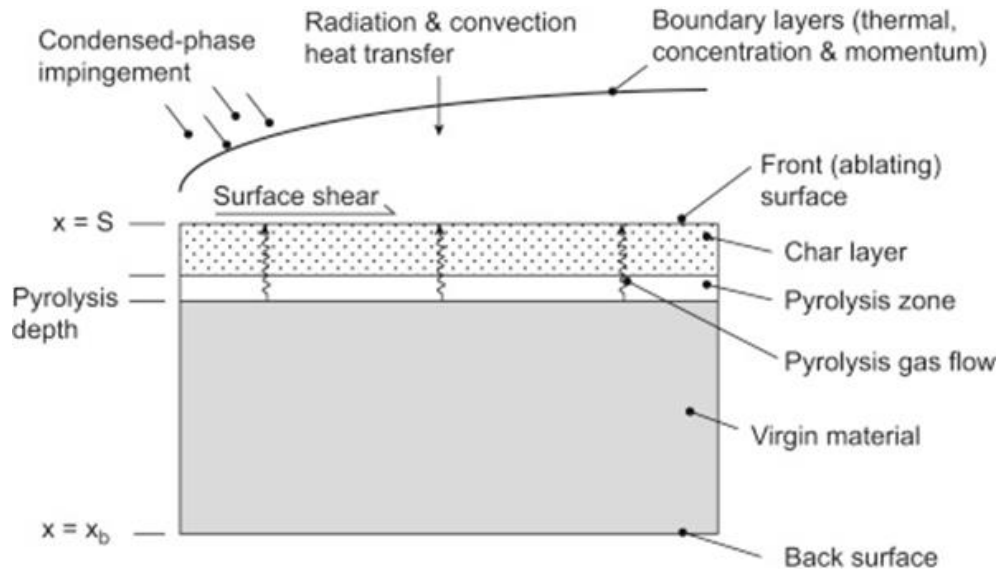


Fig. 2: Diagram of the Ablation Process.

Ablative materials purposefully undergo chemical reactions at high temperatures which release gases due to evaporation of the material around the craft. This process is helpful in a few different ways. First, the chemical reactions occurring will take heat in reducing the overall temperature. Secondly, the gas will physically carry heat away with it as it escapes. Finally, the gases create a boundary layer around the heatshield furthering the heat resistance of the material as it deteriorates. The biggest flaw of ablating materials is that they can only be used once since they oxidize. Most ablative materials have some carbon in them, so as the material oxidizes, it will leave behind charred carbon which is a strong temperature resistant material. Most heat shield materials also contain graphite, which is the material used in pencils. Surprisingly, the common material is extremely temperature resistant and can withstand temperatures of above 1,500°C. The problem with graphite is that it oxidizes quickly so the material must be coated with silicon to prevent it from contacting the atmosphere. The most common ablating material used for heat shields is Phenolic-Impregnated Carbon Ablator (PICA). PICA was developed by NASA to be used for the heatshield of the Stardust Return Capsule in 1980. This material has a low density and a low weight but has a very efficient ablative capability. Since this material is carbon based, the material will char away and leave a carbon layer on the exterior. This also means that the heatshield will only be able to be used once. Fig. 3 shows a photo of the Stardust Return Capsule before flight without any char and after reentry that is completely charred [12]. Therefore, since the mission requires no re-use of materials, PICA will be used for the heat shield.

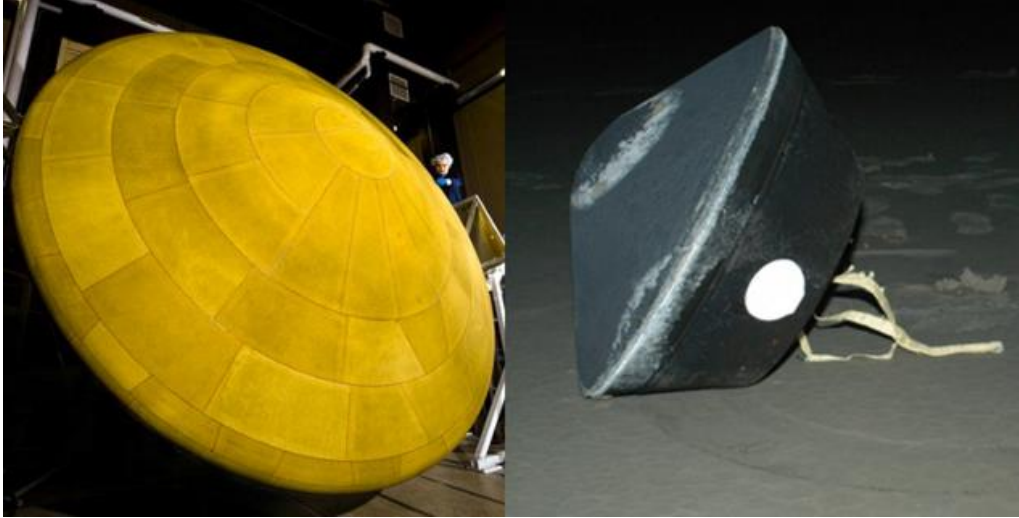


Fig. 3: Stardust Return Capsule After Reentry.

The internal makeup of the craft must also be taken into consideration since the mechanical loads experienced in reentry are extreme. Like previously stated, spacecraft undergo extreme amounts of energy whilst entering the atmosphere of a planet, upwards of 13 megajoules to be specific. In any type of flight, especially space flight, it is imperative to have the lightest weight materials possible. A material might have the strength rating required to be used in the makeup of a craft but be too heavy to be used. The bodies of most craft are made from aluminum or titanium depending on how much load the specific area will experience. The use of Computational Fluid Dynamics and other topology optimization tools allows for engineers to understand where loads should be the highest, furthering the ability to make a craft as light as possible and still withstand the loading of interplanetary travel. Therefore, the body of the craft will be made from aluminum and titanium depending on the mechanical loads occurring. Finally, the nose cone of the craft must be considered. The nose cone is possibly one of the most important parts of a craft since it endures the brute of the force of atmospheric entry. To combat these extreme forces, reinforced carbon-carbon (RCC) is typically used. RCC is a composite material that consists of a matrix of graphite reinforced with carbon fiber. This composite material was mentioned previously and consists of high strength carbon and temperature resistant graphite. Concluding the discussion on materials and aerothermodynamic phenomena, spaceships undergo extreme temperatures and pressures that require extreme materials to withstand the extremes they must endure.

V. Flight Conditions and Associated Ground Testing Parameters

The 2012 and 2020 Mars Science Laboratory, entry descent and landing system (MSL, EDL) objectives shared many of the same structural features as their predecessors and both were progeny of the Pathfinder vehicle [12,20]. From the Pathfinder mission of 1996 to present day, Mars exploration vehicles have been 70-degree spherical cone aeroshells consisting of a heat shield with ablative thermal protection and encapsulating back-shell. In contrast to their predecessors, MSL vehicles were significantly larger in diameter and entry masses (Fig. 6). The MSL vehicles were 4.5-meters in diameter, and had greater than 4 times the mass of the Pathfinder mission [18,19].

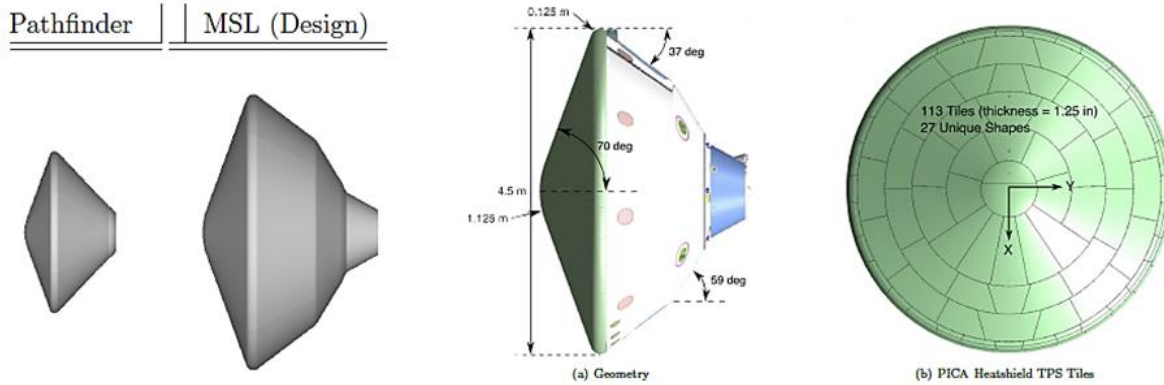


Figure 6. Geometries and comparison of the 2012 and 2020 MSL Aeroshell [12,20]

Preflight computational analysis of the 2012 vehicle concluded that the additional physical parameters would precipitate boundary layer transition (BLT) before peak heat flux [20]. This event was not recorded for other Mars missions. In addition, maximum heat flux was predicted to occur at the lee-ward shoulder of the vehicle, as opposed to the stagnation point on the windward side. Arcjet tunnel tests, performed in relation to this prediction, concluded that the traditional super lightweight ablative thermal protection system would fail. These predictive outcomes led to a change in the thermal protection system for the MSL vehicle. In addition, the unexpected location of maximum heat flux validated the addition of a heat shield sensor instrumentation suite [20].

The 2012 and 2020 MSL vehicles were upgraded to have 1.25-inch-thick thermal protection system (TPS) called phenolic impregnated carbon ablator (PICA). Further, the predicted BLT, and subsequent relocation of turbulent zones, contributed to the addition of the MSL EDL instrumentation system (MEDLI) [20]. The MEDLI data derived from the 2012 and 2020 MSL mission and suggested future ground testing is discussed below.

2020 MEDLI Data and Atmospheric Conditions

The 2020 MSL aeroshell entered the Martian atmosphere at 5.327 km/s, and a 15.38° angle of attack (AOA) [4] (Fig. 7). The size, mass and AOA of the vehicle caused aerothermal loads seen only during the 2012 MSL mission. The increased load was exacerbated by greater turbulent transitions which occurred as a result of an enlarged surface area [12]. The 2012 and 2020 MEDLI systems were designed to record aerothermal, aerodynamic, and atmospheric data events during the entry phase.

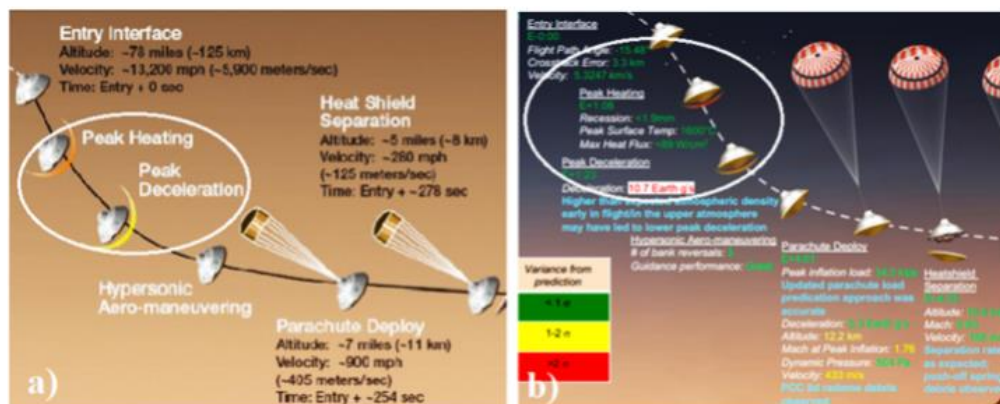


Figure 7. The (a) 2012 and (b) 2020 Peak Heating Phase of Entry for the MSL Vehicles [3,4]

The MEDLI suite was located in the interior of the MSL aeroshells and consisted of the Mars Entry Atmospheric Data System (MEADS), and the MEDLI Integrated Sensor Plug (MISP) system [3-4, 12, 20-22] (Fig. 8). The suite recorded real-time surface pressures, heat flux, and altitude during entry. It was designed to be reliable between 70 km to 10 km, at which point the heat shield, and the embedded sensors were jettisoned [4]. The 2020 MSL vehicle expanded the suite to include back-shell heat and pressure sensors. It also expanded the range and area of sensor placement, included specific hypersonic and supersonic pressure transducers, and yielded better detection of the onset of transitional flow [21-22].

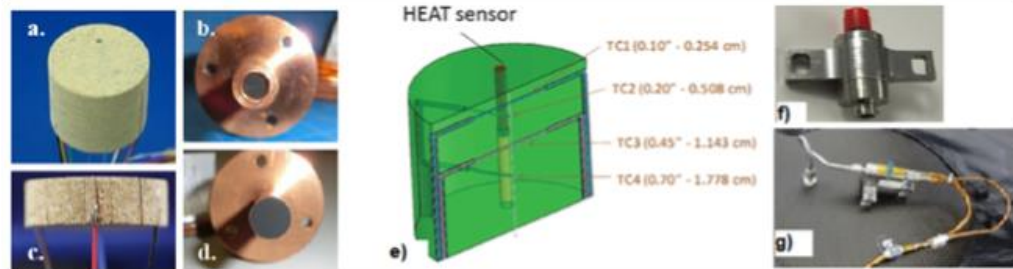


Figure 8. Ablative with embedded K- and R-type Thermocouples (a, c,e), Radiation sensor (b), Heat Flux sensors, Hypersonic and Supersonic pressure transducers (f, g) [22,21].

MEAD’s system consisted of seven embedded pressure transducers that were reliable when dynamic pressure was greater than 850 Pa [3-4]. Further, atmospheric conditions were reconstructed when data from Mars Climate Sounder (MCS), onboard Inertial Measurement Unit (IMU), and the Mars Environmental Dynamics Analyzer (MEDA) were considered. MEAD data included vehicle altitude and surface pressures, and atmospheric pressures, temperature, and densities. The MISP system included eleven K -and R-type thermocouples, heat-flux sensors, and radiation sensors (Fig. 8) [21-22]. The thermocouples and heat-flux sensors recorded surface temperatures of the TPS and radiative temperatures of the back shell [22]. In examining the data, the heatshield’s function during the 50 km to 35 km altitudes of the flight trajectory is most critical. It is this window where maximum heating occurs, maximum pressures are detected, and maximum peak deceleration happens [3-4].

Data analysis of the 2020 mission shows that prior to heat shield jettison, and hypersonic chute deployment, the MSL vehicle decelerates from 5.3247 km/sec to 0.433km/sec [4]. Simultaneously, the aeroshell dissipated more than “99% of the entry system's initial kinetic energy, mostly in the form of heat [12].” Based upon the analysis of data collected from the MEAD sensors (2012 and 2020), peak heating occurred approximately between 50 to 35 km (Fig. 9) [4, 22].

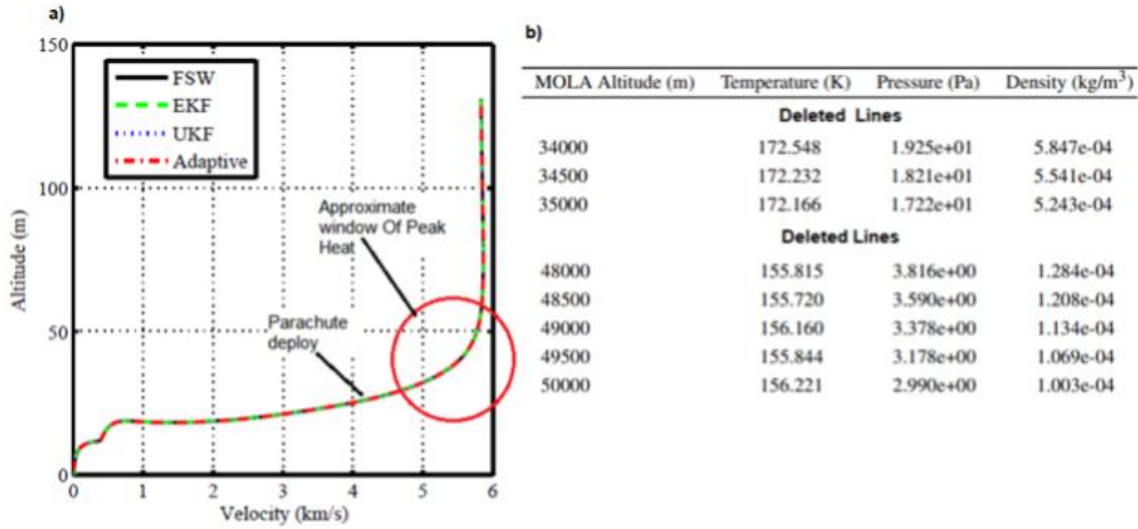


Figure 9. a) Altitude versus Velocity of 2012 MSL mission b) Static Atmospheric parameters versus Altitude of the 2020 MSL mission [3, 4, 20]

When static measures, pulled from the source shown in figure 9, was considered relative to vehicle trajectory (50 km to 35 km altitude), and Mar's gas properties, it was estimated that the 2020 MSL vehicle hit its peak surface heat and stagnation pressures between M 27.1 to M 25.7. This should have yielded calculated total -temperature between 17,193 to 17,211 K, total pressures of 1.94E9 to 7.88E9 Pa, and a total enthalpy of 14.31 MJ/kg to 14.32 MJ/kg. The total temperature, and the total pressures, are not reflected in the results. The peak subsurface temperature was approximately 1703 K while the peak stagnation pressure was 28 kPa both occurring at approximately 85 seconds after entry [3, 22]. The surface locations of the two parameters were disparate with the peak temperature occurring on the leeward side and the peak stagnation occurring in the windward side of the vehicle (Fig. 10) [12]. The discrepancies between flight-calculator values and real values may relate to missing calculations for the bow shock created during this regime. In addition, the non-equilibrium gaseous effects, radiation heat and dissipation, and the thermal properties of ablative materials are not considered here. These events are discussed throughout the literature.

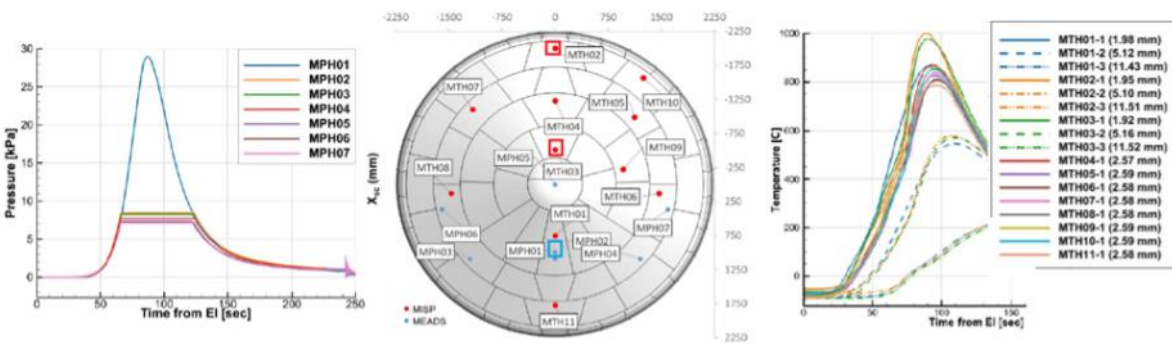


Figure 10. Maximum Subsurface Temperatures and Stagnation Pressure Location [22].

Additional analysis performed by Refs 21,22 and 12 describe boundary layer transition. This was examined in comparison to computational fluid dynamics modeling for both the 2012 and 2020 MSL missions. Seventy seconds into the entry phase, nine of eleven thermocouple sensors displayed transitional flow [22]. Moments later, the same sensors peaked in temperature. This event is shown as a slope change for the 2012 MSL mission [21] (Fig. 11). The leeside thermocouples experience a definitive increase in temperature before reaching peak temperatures at

approximately 65 seconds. This event is an attractive target for student exploration in ground testing. A brief discussion on experimental models will close this section.

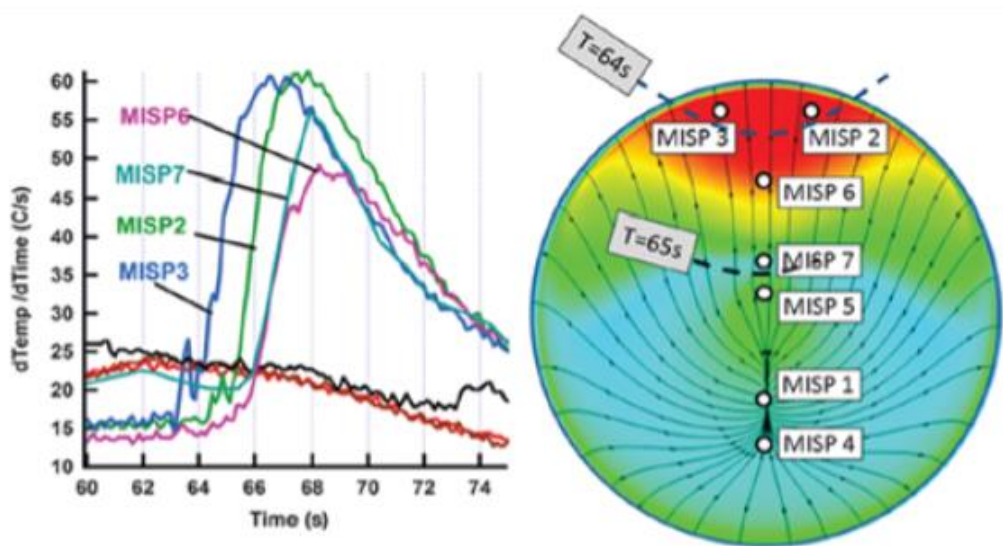


Figure 11. Boundary layer Transition in 2020 and 2012 MSL Missions. Along the Leeward Thermocouples [21].

The last observation from the MSL mission that deserves attention is the relation between computational fluid dynamic modeling and MEDLI measurements. CFD was extremely integral in modeling the aerothermal environment prior to the MSL missions. This was due to the absence of fully non-equilibrium and high-temperature tunnels [12]. The codes referenced throughout the literature include the Langley Aerothermodynamic Upwind Relaxation Algorithm (LAURA), the Data Parallel Line Relaxation (DPLR) Navier-Stokes codes, and the Fully Implicit Ablation and Thermal Response (FIAT) code. The LAURA and DPLR codes were informed by turbulent models, chemical and thermal nonequilibrium models, and radiation equilibrium models [12, 20-21]. The CFD models were highly effective at predicting surface pressures during entry but less effective at predicting surface temperature (Fig. 12) [12, 20-21]. It appears that the addition of a turbulence model that cannot account for transition may be the challenge.

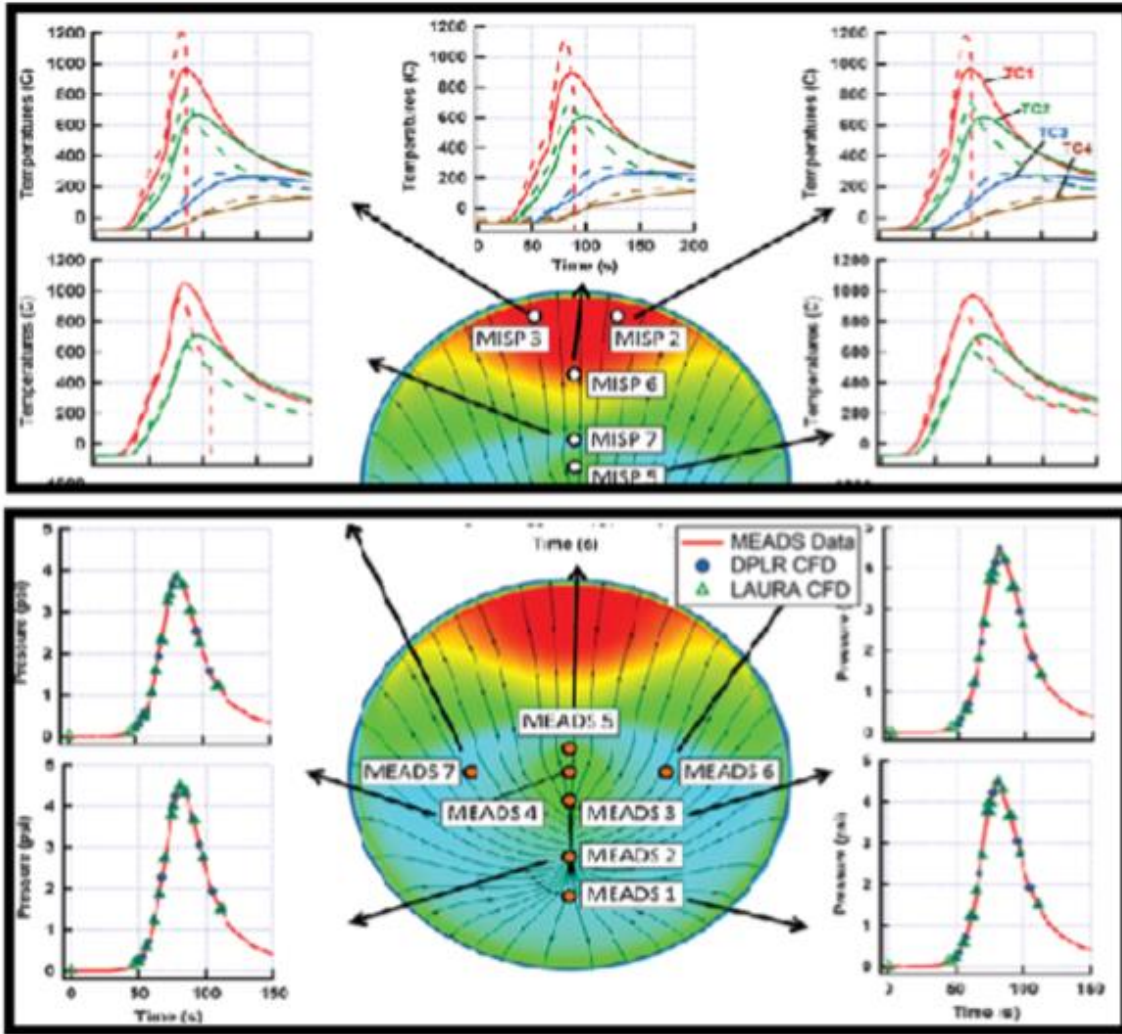


Figure 12. CFD Predictions for temperature and Pressure for the MSL Missions. (a) MISP(b) MEADS [21].

In so far as ground testing, the characterization of heat dissipation to non-equilibrium processes and a better predictive model of the boundary layer transition stands out. At present, the MSL vehicles have excess TPS to maintain a high safety factor. However, making the missions more efficient, by reducing load and improving design, predicates understanding boundary layer transition. Of the two proposed ground testing topics, better characterizing of boundary layer transition, during entry to the Martian environment, is plausible at the novice level. For example, using tunnel tests to develop an alternative to the Baldwin Lomax algebraic model or mapping transition regions on the geometry of the vehicle is imaginable. To accomplish either of these tasks, the MSL model can be placed in a variety of tunnels and conditions (Fig. 13) [20]. It seems reasonable that meaningful data can be extracted if the tilt of the model is at 16%, the test gas is CO₂ and the model is outfitted with temperature sensors. It may also be the case that simply applying novel techniques may be of benefit. Either using Planar Laser Induced Fluorescence (PLIF) or Focused-Laser Differential Interferometry (FLDI) to identify the matching characteristic frequency of transitional boundary layer flow would be a good place to start.

Table 1 Summary of BLT and turbulent heating ground tests [22–25]

Facility	Gas	D_{model} , in.	M_{∞}	$Re/ft \times 10^{-6}$	$H \times 10^{-6}$, J/kg
AEDC Tunnel 9	N ₂	6	8, 10	1.0–49.0	0.5–0.8
Langley 20 in. Mach 6	Air	6, 7, 8	6	2.0–7.5	0.2
CalTech T5	CO ₂	7	4.5	0.35–2.9	2.0–15.2
CUBRC LENS I	CO ₂	12	6.5	0.14–0.64	5.0

Figure 13. Tunnels Used to Model MSL Mission Parameters [20].

VI. Recommended Tunnels and CFD

In designing tests to simulate reentry conditions, it is important to consider what conditions are possible to be met and what must be estimated. As a spacecraft reaches the atmosphere of a planet after traveling on the order of magnitude of kilometers per second through space, there are a lot of forces and other issues that the shuttle must be able to handle if it is to be recovered. The most notable of these issues are the extremely high temperatures and high pressures, but other conditions that need to be studied are lift, drag, and transition from laminar to turbulent boundary layer.

Initial testing for the space capsule can be done in a computational fluid dynamics software (CFD). CFD can be very useful in getting approximate results on flight conditions. One problem with wind tunnels is that it is nearly impossible to match flight conditions for high speeds, such as reentry or even just supersonic flight. This is because all wind tunnels have trade-offs. An example of this is shown in Fig. 14, which displays how different types of tunnels are only able to match certain conditions and run for certain amounts of time. This is one place where CFD can become a useful tool. While CFD is generally not perfect, it has been known to yield close to experimentally tested results. In this way, CFD can be used to test some of the expected flight conditions that are not able to be tested. The best example of this is testing a high enthalpy flow at high Mach numbers for long periods of time. Given the current technology, this type of test is not possible. This means that a high enthalpy flow can be simulated over the body, and parameters such as heat transfer, pressures, and shock waves can all be studied. NASA modeled the Mars 2020 rover in CFD to show how the capsule would react in Martian reentry conditions. An image of this is shown in Fig. 15. The model shows areas of extremely high and low temperatures, with a notable peak temperature of 2500K at the surface of the rover and the heat shield at a temperature of around 1200K. This information is very important to know when designing a spacecraft because this heat transfer severely limits the materials that can be used. As a reference, 1200K would melt most types of steel.

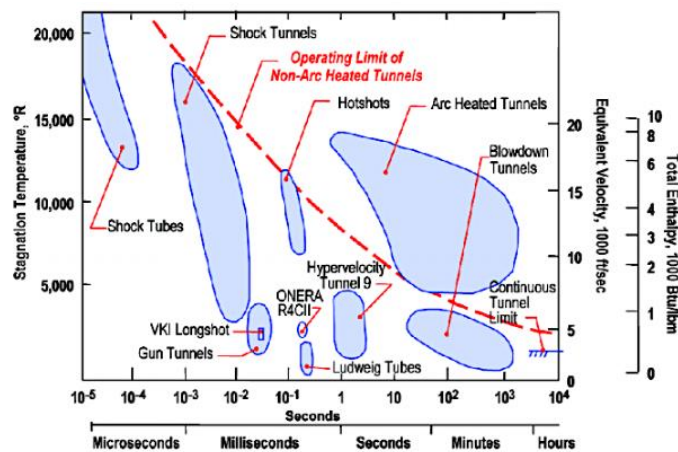


Figure 14 – Chart of different wind tunnels and their capabilities.

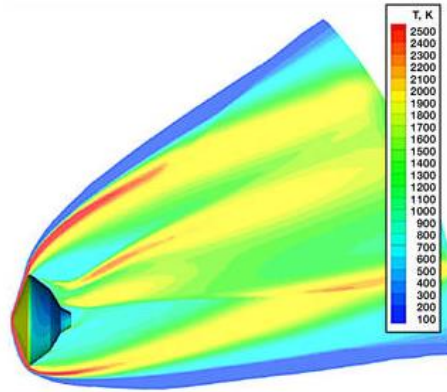


Figure 15 – NASA CFD model of the Mars 2020 spacecraft entering the Martian atmosphere [23].

For this project, it is recommended that the Data Parallel Line Relaxation code (DPLR) be used to model the flow over the body. DPLR is designed to study the aerothermodynamic heating on supersonic and hypersonic bodies that are in chemical and thermal nonequilibrium. This model has been used by NASA to study aerothermodynamic heating on its space shuttles and was awarded software of the year in 2007 [24]. However, this software is only offered to groups working either for the government or government contractors. So, another option would be to use ANSYS FLUENT CFD software to help model the shock and other aspects of the flight. This would be particularly useful in the event that a high enough Mach number cannot be reached in a wind tunnel and analysis of the shock wave is required to ensure there are no dangerous shock wave interactions on the body that could damage it.

The next recommendation for CFD code is to use it to analyze important areas on the model to see what points should have temperature or pressure sensors. CFD can be used to find points of high and low pressures and temperatures to see what areas need to be more focused on in wind tunnel testing. For example, the majority of heat transfer begins to occur when the flow transitions from laminar to turbulent in the boundary layer. CFD could be used to find these regions, and pressure and or temperature sensors can be placed just in front, on, and just behind these regions to see what effects this has on the body.

When conducting ground testing, the parameters our group is looking for are temperatures on the model, shock waves, boundary layer, and pressures on the model. To meet these conditions, it would be best to use a shock or expansion tunnel with the previously mentioned CFD. As shown in Fig. 14, shock tunnels can run at high speeds with high enthalpies. It is clearly important to try to match high Mach numbers to match flight conditions more accurately. Along with high Mach numbers, the tunnel needs to match the atmospheric conditions of Mars. The atmosphere of Mars is over 95% carbon dioxide [25]. Therefore, the tunnel must be able to hold carbon dioxide and use it as the test gas. Also, test section size should be taken into account to ensure that the model used produces the most realistic conditions. Ideally, the test section would be able to test a model the same size as the actual shuttle, but this is not always possible for high-speed wind tunnels. Finally, achieving a high Reynold's number and a high enthalpy would be ideal to help further replicate flight conditions. From these constraints, shock or expansion tunnels are the only tunnels capable of reaching these high Mach numbers and make the most sense when deciding where to do ground testing because they can also hold other gases.

The next challenge is to find the right wind tunnel to use. As expected, wind tunnels are very expensive to build, especially ones with the capabilities to handle such high Mach numbers as the ones required in this problem. However, because most tests done in a wind tunnel are to test different aspects of different flights, such as requiring different Mach numbers or different gases run through the test section, this means that running a test in a wind tunnel is not always ideal as it may not have been designed for that particular project. Therefore, it is most likely that many projects that need to be tested in a wind tunnel will have to find the wind tunnel that best fits its application, even if it is not perfect.

Luckily, this project has had many like it in the past. NASA has sent several space vessels to Mars, and all of these were tested and used CFD and wind tunnels to help design and study the vehicle before it was sent on the mission. These previous tests were done in all different ranges of tunnels for multiple parts of the missions, but the reentry portion of the mission was performed in the shock and expansion tunnels. For this project, the HYPULSE (Fig. 16) and LENS (Fig. 17) tunnels are recommended for testing the aerodynamics of the capsule and the pressures that the tunnel could experience. The HYPULSE can be a reflected shock tunnel or shock-expansion tunnel. The reflected shock tunnel setting can have higher enthalpies and is run at Mach numbers of 5 to 10, and the shock-expansion tunnel setting can have higher Mach numbers of 12 to 25 but lower enthalpies [26]. This tunnel was designed by NASA to test for re-entry and air-breathing vehicles. The tunnel can test high Mach numbers in a similar atmospheric condition as Mars by using carbon dioxide, and it can help study the heat transfer on the body. Because this tunnel was specifically designed for re-entry, it is assumed that it will work well with this project.

The other wind tunnel recommended for this project is the LENS wind tunnels. LENS is a set of wind tunnels for CUBRIC, and Fig. 18 shows the different wind tunnels and their capabilities at the LENS facility. These tunnels offer a wide variety of uses that could benefit this project by being able to test many different aspects of re-entry at the facility. The first wind tunnel to be used is the LENS I. This tunnel has a range of Mach 6 to Mach 20 with high Reynolds numbers [27], which would be great for studying aerothermal properties and has been used to study re-entry for the Gemini and Apollo missions [28]. The next recommended tunnel at this facility is the LENS XX expansion tunnel, which can have flow of up to 30,000 ft/s [27]. LENS also has a 48-inch tunnel that would work well for testing larger models.

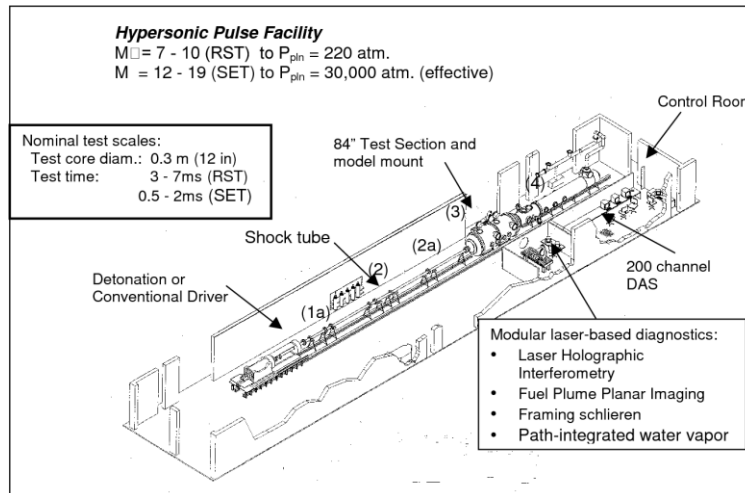


Figure 16 – Schematic of the HYPULSE wind tunnel [29].



Figure 17 – An image of the LENS tunnels [28].

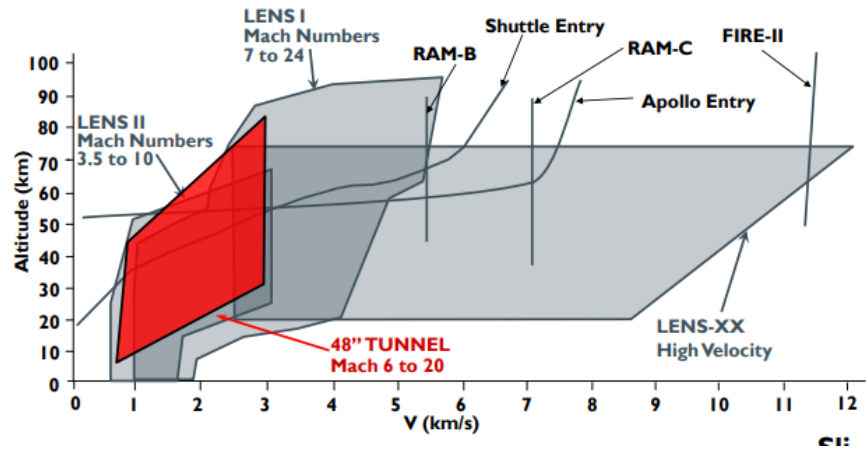


Figure 18 – Shows the capabilities of each tunnel at the LENS facility [27].

References

1. Thompson, A. (2022, January 4). *Mercury is not only the closest planet to Earth, but to every other planet in the solar system as well*. Popular Mechanics. Retrieved May 9, 2022, from <https://www.popularmechanics.com/space/solar-system/a26839314/closest-planet-to-earth-on-average/>
2. Dobrijevic, D. (2022, February 4). *Distance to mars: How far away is the Red Planet?* Space.com. Retrieved May 9, 2022, from <https://www.space.com/16875-how-far-away-is-mars.html>
3. Nasa: “Entry, descent and landing (EDL),” NASA Available: <https://mars.nasa.gov/mars2020/timeline/landing/entry-descent-landing/>.
4. Nasa1: Hall, N., ed., “Isentropic flow equations,” NASA Available: <https://www.grc.nasa.gov/www/k-12/airplane/isentrop.html>.
5. Dutta, S., and Braun, R. D., “Statistical entry, descent, and landing performance reconstruction of the Mars Science Laboratory,” *Journal of Spacecraft and Rockets*, vol. 51, 2014, pp. 1048–1061.
6. Dutta, S., Karlgaard, C. D., Kass, D., Mischna, M., Villar III, G. G., “Post-flight analysis of atmospheric properties from Mars 2020 entry, descent, and landing,” 2022 (to be published).
7. Marte: Marte, J. E., “Viscous Damping of Roll During Entry of a Mars Entry and Landing Capsule” Available: <https://ntrs.nasa.gov/api/citations/19660016857/downloads/19660016857.pdf>.
8. Nasa2: Hall, N., ed., “Normal shock wave equations,” NASA Available: <https://www.grc.nasa.gov/www/k-12/airplane/normal.html>.
9. Bose, D., White, T., Mahzari, M., and Edquist, K., “Reconstruction of aerothermal environment and heat shield response of Mars Science Laboratory,” *Journal of Spacecraft and Rockets*, vol. 51, 2014, pp. 1174–1184.
10. “Comparing the atmospheres of Mars and Earth,” ESA Available: https://www.esa.int/ESA_Multimedia/Images/2018/04/Comparing_the_atmospheres_of_Mars_and_Earth#:~:text=Mars%20is%20about%20half%20the,rich%20in%20nitrogen%20and%20oxygen. [APA1]
11. Dunbar, B., “The right stuff for super spaceships,” NASA Available: https://www.nasa.gov/vision/space/gettingtospace/16sep_rightstuff.html.
12. Edquist, K. T., Hollis, B. R., Johnston, C. O., Bose, D., White, T. R., and Mahzari, M., “Mars Science Laboratory Heat Shield aerothermodynamics: Design and reconstruction,” *Journal of Spacecraft and Rockets*, vol. 51, 2014, pp. 1106–1124.
13. Elliot, D. J., “Ablation,” *Ablation - an overview | ScienceDirect Topics* Available: <https://www.sciencedirect.com/topics/engineering/ablation>.
14. Huang, A., “Low density ablators,” NASA Available: <https://www.nasa.gov/centers/ames/thermal-protection-materials/tps-materials-development/low-density-ablators.html>.
15. “Mars physical and orbital statistics, comparisons - netscape” Available: https://meteor.geol.iastate.edu/classes/mt452/Class_Discussion/Mars-physical_and_orbital_statistics.pdf. [retrieved 11 April 2022]
16. “Perseverance rover decelerates in the martian atmosphere,” NASA Available: <https://www.jpl.nasa.gov/images/pia24314-perseverance-rover-decelerates-in-the-martian-atmosphere-illustration>.
17. Loff, S., “NASA images,” NASA Available: <https://www.nasa.gov/multimedia/imagegallery/index.html>.
18. “Mars entry instrumentation flight data and Mars 2020 Entry Environments,” *AIAA SCITECH 2022 Forum, 2022*
19. Getting to Mars,” NASA Available: <https://mars.nasa.gov/msl/spacecraft/getting-to-mars/>. “Mars Pathfinder fact sheet,” NASA Available: https://mars.nasa.gov/MPF/mpf/fact_sheet.html.
20. Edquist, K., Dyakonov, A., Wright, M., and Tang, C., “Aerothermodynamic design of the Mars Science Laboratory heatshield,” *41st AIAA Thermophysics Conference*, 2009.
21. Bose, D., White, T., Mahzari, M., and Edquist, K., “Reconstruction of aerothermal environment and heat shield response of Mars Science Laboratory,” *Journal of Spacecraft and Rockets*, vol. 51, 2014, pp. 1174–1184.
22. White, T. R., Mahzari, M., Miller, R. A., Tang, C. Y., Karlgaard, C. D., Alpert, H., Wright, H. S., and Kuhl, C.,
23. Vitug, E. (2020, April 7). *Entry systems modeling (ESM)*. NASA. Retrieved May 9, 2022, from https://www.nasa.gov/directorates/spacetech/game_changing_development/projects/ESM/
24. *NASA's DPLR named software of the Year*. NASA's DPLR is Software of the Year. (n.d.). Retrieved May 9, 2022, from http://www.gridgen.com/applications/dplr_soy.shtml
25. Dobrijevic, D. (2022, February 25). *Mars' atmosphere: Facts about composition and climate*. Space.com. Retrieved May 9, 2022, from <https://www.space.com/16903-mars-atmosphere-climate-weather.html>
26. Erdos, J. I., Bakos, R. J., Castrogiovanni, A., & Rogers, C. R. (n.d.). *Dual Mode Shock-Expansion/Reflected-Shock Tunnel*. Retrieved May 9, 2022, from <https://ntrs.nasa.gov/api/citations/20040100806/downloads/20040100806.pdf>.

27. Holden, M. S. (n.d.). *DTIC*. The LENS Facilities and Experimental Studies to Evaluate the Modeling of Boundary Layer Transition, Shock/ Boundary Layer Interaction, Real Gas, Radiation and Plasma Phenomena in Contemporary CFD Codes. Retrieved May 15, 2022, from <https://apps.dtic.mil/sti/pdfs/ADA588962.pdf>
28. User, S. (n.d.). Lens 48-inch mach 6 to 18 shock tunnel. Retrieved May 15, 2022, from <https://www.cubrc.org/index.php/aerothermal-aero-optic-evaluation/lens-48-inch-mach-6-to-18-shock-tunnel>

Rogers, R. C., & Shih, A. T. (2001). *37THAIAA/ASME/SAE/ASEE Joint Propulsion conference & Exhibit - NASA*. Scramjet Tests in a Shock Tunnel at Flight Mach 7, 10, and 15 Conditions. Retrieved May 15, 2022, from <https://ntrs.nasa.gov/api/citations/20010083962/downloads/20010083962.pdf>